Calculations of Non-Metallic Particles Removal from Liquid Aluminium to Top Slag

P.L. Żak [a], * (iD) **, K. Kuglin** [b] **, M. Szucki** [c] (iD) **, D. Kalisz** [a] (iD) **, N. Mrówka** [d] **, E. Dan** [d]

[a] AGH University of Krakow, Krakow, Poland
[b] NPA Skawina Sp. z o. o., Poland
[c] Technische Universität Bergakademie Freiberg, Germany
[d] no affiliation
* Correspondence contact: e-mail: pawelzak@agh.edu.pl

Abstract

In the paper, the results of a numerical analysis of KCl and KF particles present in liquid aluminium assimilation to the slag are presented. The authors analysed particle movement in the slag model, which is based on buoyant, capillary, viscosity, Newton and repulsion forces, interfacial tensions at the interface of phases and surface energy during the particle movement through phases boundary. On the basis of the mathematical model, a computer programme was written to make simulations under different conditions. The results of particle position in the slag are presented for different particle radiuses: 1, 5, 10, 20 μm, and constant viscosity of the slag including velocity evolution of the velocity. Another approach was used to indicate the influence of slag viscosity on particle and slag penetration depth. During computations, selected viscosities of slag of 0.0012, 0.0015, 0.0018 [kg/m·s] were taken into account. Different comparisons were made for the chosen particle sizes. Each examination takes into account the impact of the particle type. The results clearly show that for larger particles the penetration depth is greater and viscosity of the slag has an impact on the velocity evolution during assimilation process.

Keywords: Numerical simulation, Liquid aluminium, Particle motion, Inclusions

1. Introduction

Inclusions present in liquid aluminium, including unwanted gases (hydrogen), alkali metals (lithium and sodium), alkaline earth metals (magnesium and calcium), and inclusions (oxides, borides, nitrides, carbides, and chlorides), can cause serious defects when critical values of their content are exceeded. Among their sources are: alumina, which is a substrate in the process of aluminium production from bauxite, electrolyte components from electrolysis, carbon anode, refractory lining of metallurgical units, and subsequent refining processes [1,2].

In industrial practice, several refining steps are usually combined, such as blowing of inert gas, refining powders, and filtration. Aluminium refining methods involve techniques that make us refining powders, such as aluminium fluoride (AlF_3) or magnesium chloride ($MgCl_2$) added to melted aluminium [3-7], salt – a mixture of sodium chloride (NaCl) or potassium chloride (KCl) and calcium fluoride, or aluminium fluoride or cryolite applied to the surface of liquid metal [8-13]. When the liquid metal bath is stirred with an inert gas, the liquid aluminium, gas bubbles, and non-metallic particles are moved toward the surface. The removal process can be divided into three stages: buoyancy of the particle phase to the interfacial division boundary, penetration through the interfacial division boundary, dissolution in the liquid refiner, or removal directly to the atmosphere. Stage 2, presented in the present work, is an important element in the refinement, which is

to guarantee the required purity of liquid aluminium or its alloy. If a given inclusion gets close to the liquid aluminium-melted refining agent (flux) interface, then the physicochemical parameters of the particle-liquid-metal-flux system will determine whether a given particle is permanently expelled from the liquid metal or not. In the course of this process, several phenomena relating to the behaviour of the particle may take place, e.g., flowing out, repulsion, absorption, and oscillation at the liquid metal/coating layer interface [10, 13-16].

The parameters that determine the removal efficiency of particle will be the viscosity of the the layer on top of liquid metal, the densities of the particle and the fluid, as well as the interfacial tensions at the interface of the three phases [4, 15-21]. One of the most important parameters determining the effectiveness of the removal of particles from the slag is its viscosity. Figures [1 - 4] show the viscosity isotherm lines for selected bicomponent flux systems used for aluminum refining [11]. It follows that at Al_2O_3 content of 0-9.8%, the viscosity of the investigated Na_3AlF_6 Al_2O_3 system varies in a minimal range. An intense increase in viscosity is observed at about 15 wt.% Al_2O_3 content. In the case of the Na_3AlF_4 - Li_3AlF_6 system, the viscosity isotherms reach their minimum at the Li_3AlF_6 content of approximately 60 wt%, similar isotherms are observed for the system. Na_3AlF_4 – LiF system. The special importance is that this case is presented for the Na_3AlF_4 NaCl system, where viscosity decreases with the addition of NaCl [11].
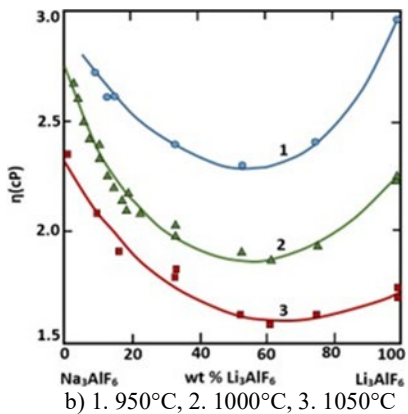

a) 1. 1000°C, 2. 1050°C
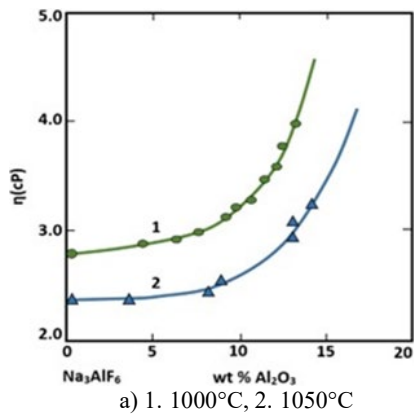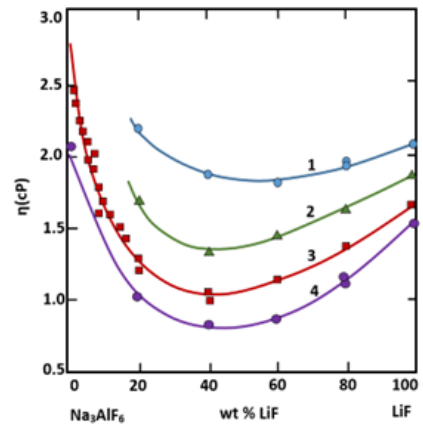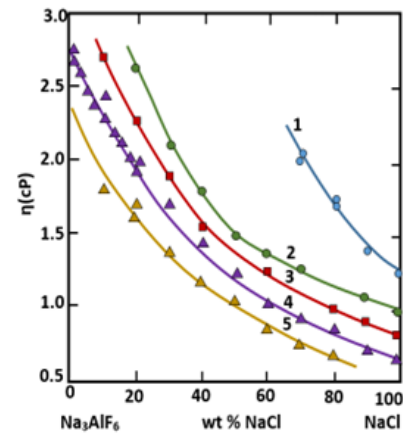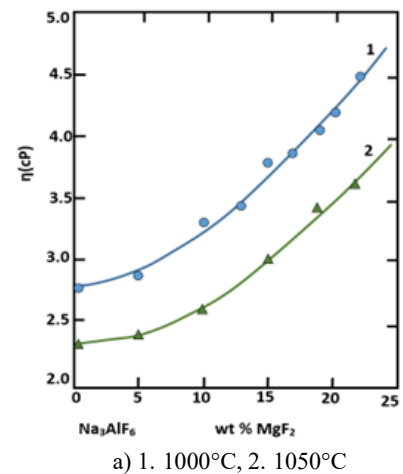

b) 1. 950°C, 2. 1000°C, 3. 1050°C
Fig. 1. Viscosity isotherms of the melted mixtures:
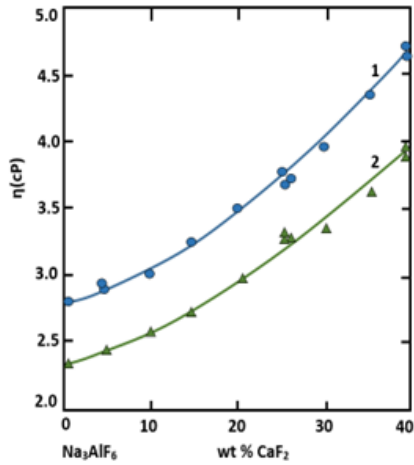(a) Na_3AlF_6 – Al_2O_3, (b) Na_3AlF_6 – Li_3AlF_6 [11]

a) 1. 900°C, 2. 950°C, 3. 1000°C, 4. 1050°C

b) 1. 850°C, 2. 900°C, 3. 950°C, 4. 1000°C, 5. 1050°C
Fig. 2. Viscosity isotherms of the melted mixtures:
(a) Na_3AlF_6 – LiF, (b) Na_3AlF_6 – NaCl

a) 1. 1000°C, 2. 1050°C

b) 1. 1000°C, 2. 1050°C

Fig. 3. Viscosity isotherms of the melted mixtures:
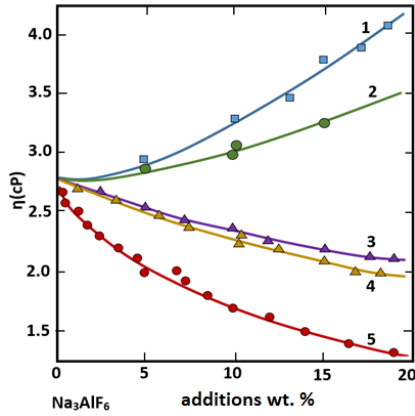(a) $Na_3AlF_6 - MgF_2$, (b) $Na_3AlF_6 - CaF_2$

Fig. 4. Impact of different additions on the viscosity of cryolite
at 1000 ° C temperature; Numbers denote different additions:
1.MgF_2, 2. CaF_2, 3. Li_3AlF_6, 4. NaCl, 5. LiF

2. Mathematical Model Equations

The movement of the particle within the slag during assimilation phenomena is described by the set of equations that will be presented in the following paragraph.

The buoyant force, F_W is given by equation (1), [9]:

$$F_W = \frac{4}{3} \cdot R^3 \cdot \left(\Delta_b \cdot \rho_S - \rho_W\right) \cdot g \tag{1}$$

where Δ_b is the value that can be calculated using expression:

$$\Delta_b = \frac{1}{4} \cdot \left(\frac{\rho_M}{\rho_S} - 1\right) \cdot \left(\frac{Z}{R}\right)^3 - \frac{4}{3} \cdot \left(\frac{\rho_M}{\rho_S} - 1\right) \cdot \left(\frac{Z}{R}\right)^2 + \frac{\rho_M}{\rho_S} \tag{2}$$

where:

ρ_M - alloy density [kg/m^3],
ρ_W - particle density [kg/m^3],
R - radius of the particle [m],
g - gravity acceleration [m/s^2],
Z - particle position coordinate [m].

The capillary force [9] can be calculated from:

$$F_\sigma = \left(-2 \cdot \pi \cdot R + 2 \cdot \pi \cdot Z\right) \cdot \sigma_{MS} + 2 \cdot \pi \cdot R \cdot \sigma_{WS} - 2 \cdot \pi \cdot R \cdot \sigma_{WM} \tag{3}$$

where:

σ_{MS}, σ_{WS}, σ_{WM} - interfacial tensions at the interface of phases: MS for metal – slag, WS for particle – slag, WM for particle – metal, [J/m^2].

The viscosity force is given by equation (2), [9]:

$$F_{VIS} = 6 \cdot \pi \cdot R \cdot \eta_S \cdot B \cdot \frac{dZ}{dT} \tag{4}$$

where B value depends on the value of $\frac{Z}{R}$ ratio:

$$B = 1 \text{ for } \frac{Z}{R} \geq 1 \tag{5}$$

$$B = \left(\frac{\eta_M}{\eta_S} - 1\right) \cdot \left(\frac{Z}{R}\right)^2 - 2 \cdot \left(\frac{\eta_M}{\eta_S} - 1\right) \cdot \left(\frac{Z}{R}\right) + \frac{\eta_M}{\eta_S} \text{ for } 0 \leq \frac{Z}{R} \leq 1 \tag{6}$$

and η_S, η_M parameters denote slag and alloy viscosity [Pa·s] respectively.

The added mass force:

$$F_m = \frac{1}{2} \cdot \frac{4}{3} \pi \cdot R^3 \rho_S \Delta_b \frac{d^2 Z}{dt^2} \tag{7}$$

where the parameter t denotes the time [s]

The buoyant force, F_W (1), among others, depends on the position versus surface that separates phases. This position is denoted by the Z variable and may have positive or negative values. For particle that crosses the surface Z variable is positive. The capillary force, F_σ (3), is related to the value of surface tension. As particle moves vertically, force change sign. Usually the surface tensions at the particle-metal and particle-slag hold the relation: σ_{WM} σ_{WS}, if this condition is fulfilled, the particle travels from metal to slag. As critical values of surface areas wetted by slag and metal are reached, the direction of capillary force changes, and this force starts to counteract the process of moving precipitation particle from metal to slag. The value of the capillary force depends on the chemical composition of the metal alloy and the slag [10,13-14]. Another force that has an impact on the position of the precipitation particles is the viscosity force, F_{VIS} (4).

This force value depends on the viscosity of metal and slag, and their impact on the movement through interfacial boundary, impact of mentioned viscosities on the viscosity force is gathered in the value of coefficient B. This coefficient value changes during the particle movement with the change in the precipitation position Z.

Another force, F_m (7), represents the added mass force, as a result of Newton's second law of motion.

The F_{rep} (9) is the the repulsion force that is result of the resistance of the slag surface to the assimilation of particles. The value of the surface energy, E, during the movement through phases boundary is given by equation (8):

$$E = -\pi (2 \cdot R - Z - Z^2) \cdot \sigma_{MS} + 2\pi \cdot R - Z \cdot \sigma_{WS} + 2\pi \cdot R \cdot (2 \cdot R - Z) \cdot \sigma_{WN} \tag{8}$$

As the particle crosses the phase boundary, the energy changes. This phenomenon is related to the particle - slag in the surface change of the contact area, the particle - metal and metal – slag. As a result, repulsive force appears, which inhibits particle movement into the slag.

The repulsion force [10]:

$$F_{rep} = \frac{dE}{dZ} = 2\pi \cdot R \cdot \sigma_{MS} - \frac{Z}{R} - 1 - cos\theta \tag{9}$$

The cosinus angle can be calculated on the basis of the interfacial tensions ratio:

$$cos\theta = \frac{\sigma_{WM} - \sigma_{WS}}{\sigma_{MS}} \tag{10}$$

3. Methodology of numerical approach

Within described research computer programme that was based on above equations 1 - 10 was prepared by the authors. It allows to prepare simulation of non-metallic particle behaviour at the aluminium alloy – top slag boundary. The block diagram which shows calculation algorithm is shown in Fig. 5. The computer program was prepared in the C++ programming language as a console application. The input and output data are stored in files, which format is a strict set. Each line of input file refers to different input parameters, and numerical model inputs are also gathered in the file. Lines consists of three parts, user-friendly parameter description, parameter value, and unit. The mentioned parts are separated by space symbol. The first line has output data names, again separated by space symbol. The following lines consist of values only; there is no more text in the file, and the values are separated by space. Such construction of the output file allows it to be easily used in a spreadsheet. After starting the computer programme finds the input file and initiates inner variables with proper values. The output file is also initiated at this point. Some initial values are calculated on the basis of input data from input file, those values are contact angle (11) and particle initial velocity:

$$V_0 = \frac{2}{9} \cdot R^2 \cdot g \cdot \frac{\rho_M - \rho_W}{h_M} \tag{11}$$

Further, computational loop starts, time step is set in the input file. Values of forces are computed. Base of this values and Newton's Second Law of Motion differential equations are prepared. This set of Ordinary Differential Equations (ODEs) is solved using Runge-Kutta 4th order method. At given times (calculated on the base of time step length) data is added to output file. Computations are stopped when end of computation time is reached or whole particle is in the slag. After fulfilling the end condition for the computational loop all disk files are closed and computer program terminates.
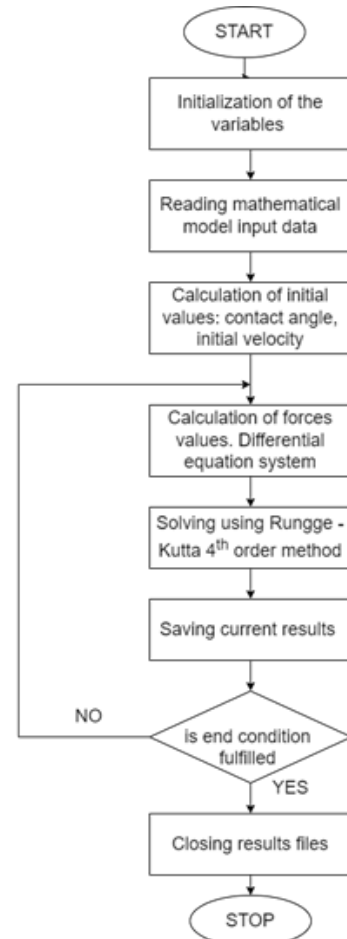

Fig. 5. The block diagram of the computer program for simulation of particle behaviour on the phase boundary

Calculations of the particle velocity and trajectory at the phases boundary was performed for different initial radiuses under spherical particle shape assumption, radius of the particle was changed in the range 1 - 20[μm]. During simulations two types of particles were taken into account: KF and KCl, physical data for each of the non-metallic particles are gathered in the table 1.

Table 1.
Data for non-metalic particles used for simulation [8-9, 22]

Particle type	Density ρ	Surface tension σ_{WM}	Surface tension σ_{WS}	Surface tension σ_{MS}
Units	[kg/m^3]		[N/m]	
KF	2480	0.5	0.05	0.28
KCl	1980	0.792	0.0792	0.28

4. Results and discussion

Simulations lead to the determination of the position of the particle versus the surface of the slag. Obtained results are presented in the form of figures. In the figures, selected combinations of the results are collected. The figures presented may be divided into two groups: first, the velocity and position of KCl and KF particles in time are compared, and the second group shows the varying viscosity impact on the KCl particles and KF particles behaviour when travelling into the slag.

In figures 6 - 9 plots of the position in the slag are shown for different particle radiuses: 1, 5, 10, 20 μm. Calculations were made under the assumption that the viscosity of the slag is equal to 0.0015 [kg/m·s]. As the coordinate H (depth of penetration of the slag by the particle) increases, the particle travels through into the slag layer. This fact was noted for all analysed cases. Growth of the H coordinate means that the particle is moving into slag. Growth of this line depends on the characteristic of movement and changes in time. If the movement of the particle stops – horizontal line in plot, it means that it was absorbed by the slag.

Analyse of the results presented in figures 6 - 9 allows to state that for the particles of greater radiuses, depth of slag layer penetration is deeper. In the case of 1 μm particle penetration depth is in the range of 1.6 – 2 μm. In the case of 20 μm particle penetration depth is in the range of 33 – 40 μm. Taking into account the depth of variation of the particle size is similar as one scales it to the size multiplication factor.

Another observation can be made on the influence of the non-metallic particle type on a particle movement. In the case of the KCl particles, a different behaviour can be seen than for the KF particles. The KCl particles travel through the slag faster, but their penetration is not as deep as calculated for KF particles. The velocity, U, plots for different sizes of particles prove that the penetration rate for different non-metallic particles differs significantly. The KCl particle moves with high velocity at the beginning of the process and then slows down rapidly. In the case of KF particle, for a long time since beginning of the process, the velocity is about similar value. Then it is decreased to zero. Similar observations can be made for all sizes of particles that were taken into account: 1, 5, 10, 20 μm. In the case of KCl particles the velocity in the slag is much higher than the velocity of KF particles at the beginning of the process. But as they slow down they velocity approaches zero very fast, while KF particles still have relatively high velocity. In comparison with results presented in figures 6 - 9, this explains why the slag penetration of KF particles is deeper than that of KCl.
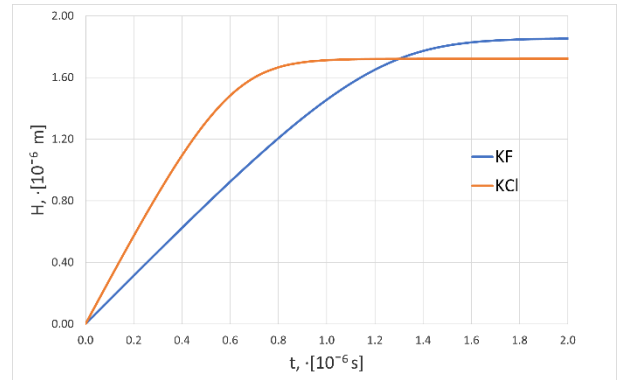

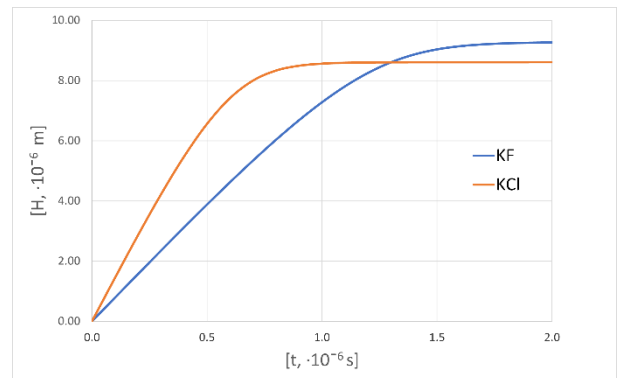Fig. 6. Non-metallic particle of 1 μm position versus slag – metal surface

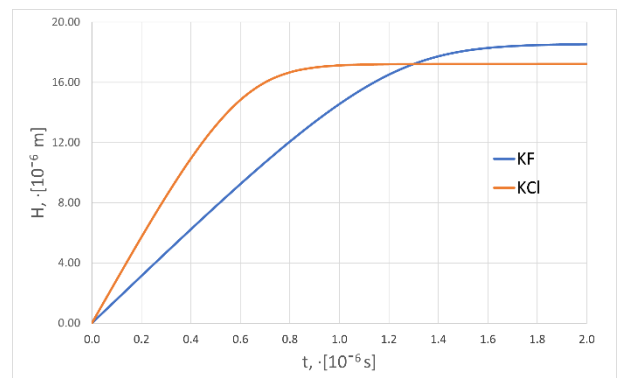Fig. 7. Non-metallic particle of 5 μm position versus slag – metal surface

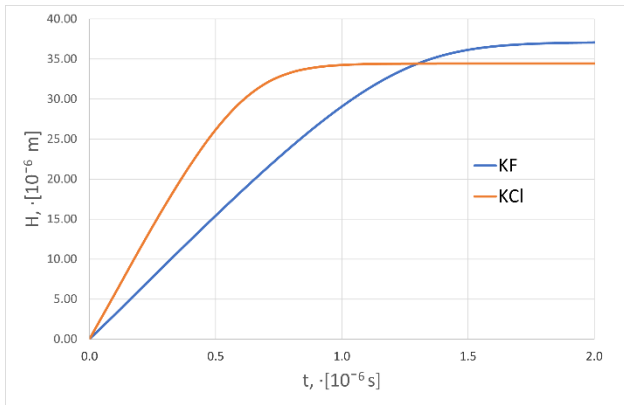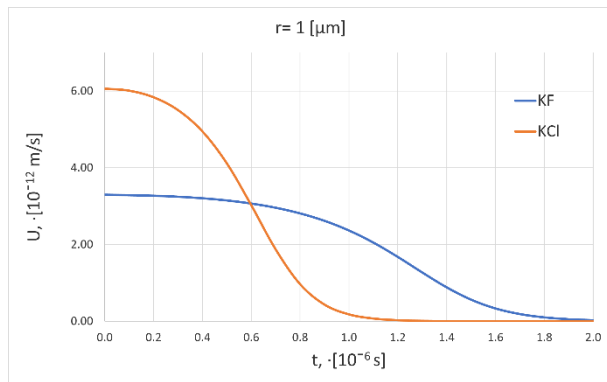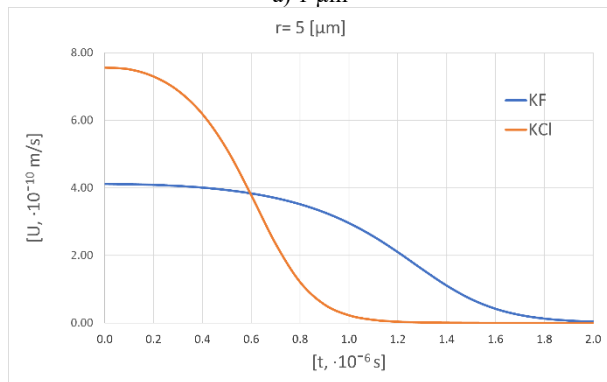Fig. 8. Non-metallic particle of 10 μm position versus slag – metal surface
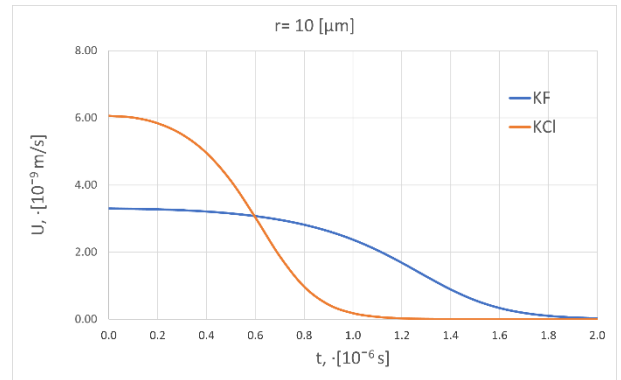
Fig. 9. Non-metallic particle of 20 μm position versus slag – metal surface
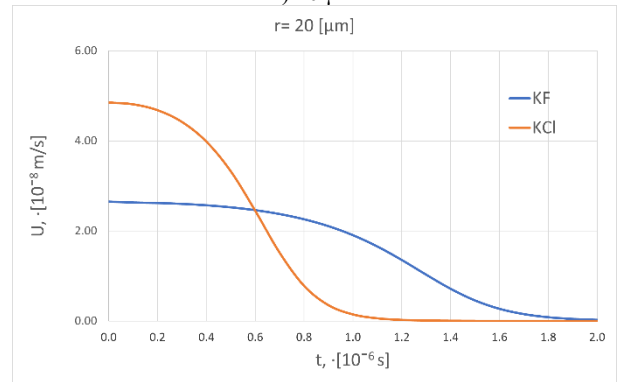

a) 1 μm

b) 5 μm

c) 10 μm

d) 20 μm

Fig. 10. Velocity of different size particles while travelling within the slag. Sizes of particles used for calculations: (a) 1 μm, (b) 5 μm, (c) 10 μm, (d) 20 μm

The size of non-metallic particles also impact on the velocity. In general, the larger particles move faster in the slag. This observation can be made for both types of particles. This result is consistent with previous results of particle position in the slag. The larger particles penetrated the slag deeper than the smaller particles (Figures 6 - 9). The time of particle assimilation by the slag is more or less the same. The process ends when the particle position line becomes horizontally flat in particle position versus slag – metal surface plots. The velocity plots (Fig. 10) allows to analyse movement rate of the particle; in this case assimilation process ends where velocity value equals zero.

Another subject of this study was to analyse the viscosity of the movement of slag impact on the particles in the slag as well as it's assimilation by the slag. Results for the selected particle radius are presented in Figures 11 and 12. Figure 11 shows a comparison of the particle position change in time for KCl and KF particle and for different values of slag viscosity. The radiuses of the compared particles are 5 and the 20 μm and selected slag viscosities are: 0.0012, 0.0015, 0.0018 [kg/m·s]. It can be noted that for higher values of viscosity particle travelling rate is slower. The curves for the radiuses analysed and values of viscosity are similar. However, for greater viscosity values curves are less rounded.
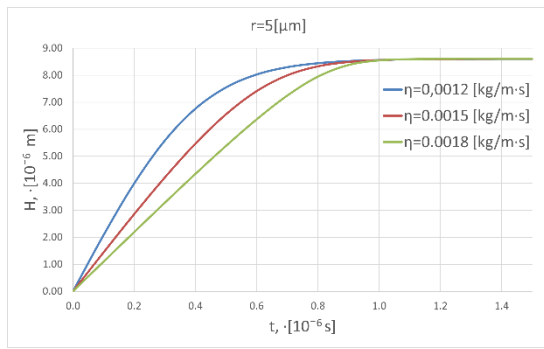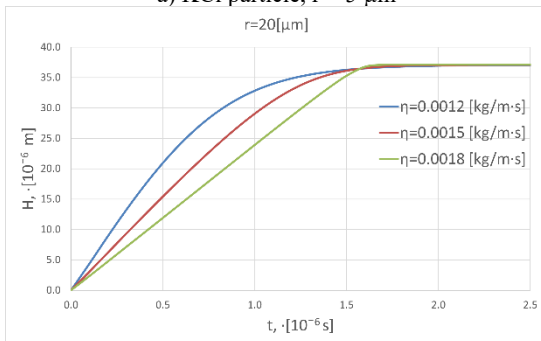
a) KCl particle, r = 5 μm
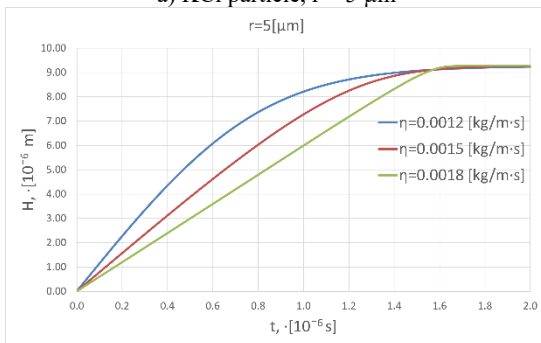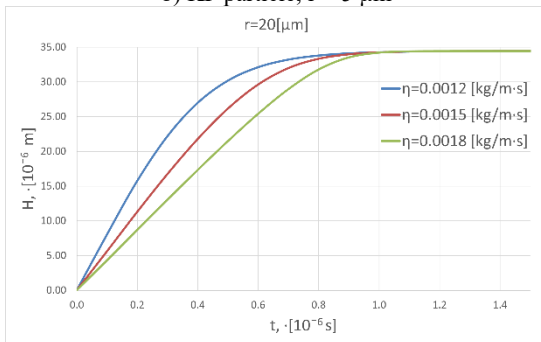
b) KF particle, r = 5 μm

a) KCl particle, r = 5 μm
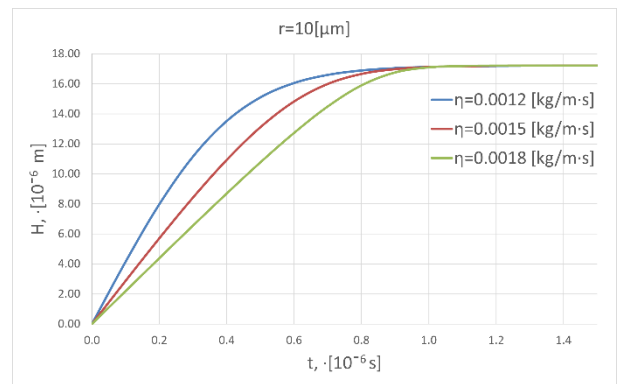

b) KF particle, r = 5 μm

Fig. 11. Position of the particles in the slag for different particle sizes: 5, 20 μm and different particle types: KCl and KF particles

The particle movement in the slag is slower and is visible on the curve. The curves for the KCl particle are more rounded than

for the KF particle. For the viscosity value equal to 0.0018 [kg/m·s] curve is similar to two lines that are joined smoothly at a very short distance. The results show that penetration depth in the case of KCl particles is not as deep as in the case of KF particles, but this difference value is not large. It became greater for the particles of a larger radius.

In Figure 12 the change of the position of the particle in the slag and change of its velocity during the process are shown for different viscosities of the slag. Calculations were made for both types of non-metallic particles KCl and KF of chosen radius of 10 μm. It can be seen that for low values of slag viscosity the travel speed at the beginning of the process is greater but slows down very fast. In the case of higher viscosities at the beginning of the process, the velocity is not as large as in the previous case, however, its value is stable at this level for a longer period of time. For high viscosities, the case of high viscosities 0.0018 [kg / m·s] velocity for long time is almost constant.
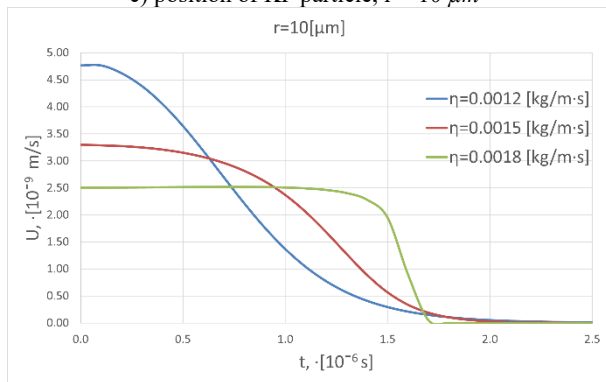

a) position of KCl particle, r = 10 μm
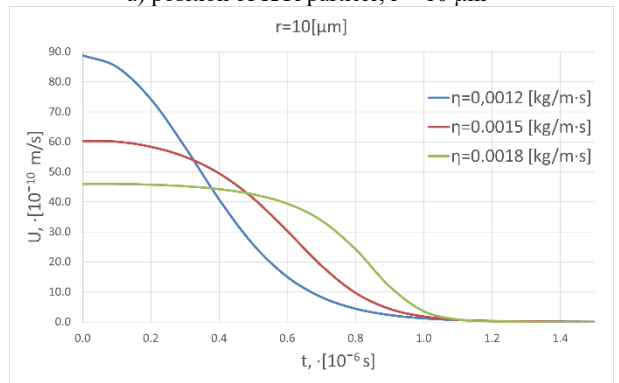
b) velocity of KCl particle, r = 10 μm
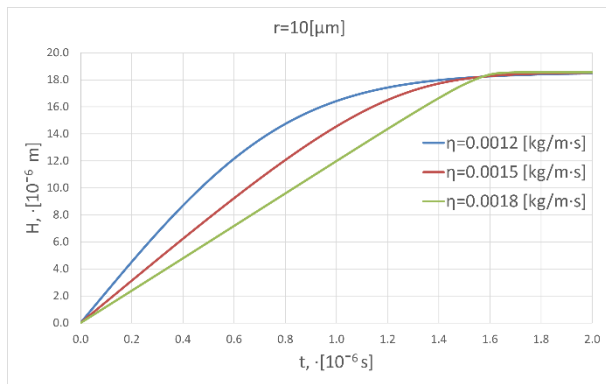
c) position of KF particle, r = 10 μm

b) velocity of KF particle, r = 10 μm

Fig. 12. Position, H, and velocity, U, of different type particles of 10 μm radius in slag. Plots for KCl particles are labelled (a), (b) and plots for KF particles (c), (d).

Calculated velocities for KCl particles are greater than for KF particles, and for both particle types the depth of penetration is similar. This is due to the movement time in the slag, which is longer for KF particles than for KCl particles.

4. Conclusions

1. In terms of paper size and type of non - metallic particle, the influence of slag viscosity on the particle assimilation process toslag was examined. The presented discussion of the obtained results leads to the following conclusions:
2. During a particle assimilation into slag, the depth of penetration of the slag layer depends on particle radius and the non-metallic particle type. The greater the particle radius, the deeper the penetration depth. In the analysed cases, KF particles went deeper into the slag layer than KCl particles.
3. The values of the velocity of the particles are also dependent on its radius. For the greater particles, the velocity value is greater. The velocity changes during the assimilation process; its change characteristic depends on the particle type.
4. It can be seen from the velocity curves stage of the assimilation process. When the particle velocity is equal to zero, the assimilation process ends.

5. During the viscosity of the examination, three values of the slag were taken into account: 0.0012, 0.0015, 0.0018 [kg / m·s]. Viscosity values have the great impact on a particle velocity characteristic during the assimilation process. For smaller viscosity values, velocity at the beginning of the process is greater, but it slows down rapidly. For greater viscosity values, the velocity at the beginning of the process is smaller, but it is almost constant for a long period of time before it starts to slow down.
6. Impact of slag viscosity on the slag penetration depth of penetration of the non-metallic particle depends on its type. In the case of KCl particles of the same size, the penetration depth is more less the same. In the case of KF particles of the same size, penetration depth is deeper for greater viscosity values. However, these differences are rather insignificant.

Acknowledgements

References

[1] Instone, S., Buchholz, A. & Gruen, G. U. (2008). Inclusion transport phenomena in casting furnaces. *Light Metals (TMS).* 811-816.

[2] Prillhofer, B., Antrekowitsch, H., Böttcher, H. & Enright, P. (2008). Non-metallic inclusions in the secondary aluminium industry for the production of aerospace alloys. *Light Metals (TMS).* 603-608.

[3] Johansen, S.T., Gradahl, S. & Myrbostad, E. (1996). Experimental determination of bubble sizes in melt refining reactors. *Light Metals (TMS).* 1027-1031.

[4] Johansen, S.T., Robertson, D.G.C., Woje, K. & Engh, T.A. (1988). Fluid dynamics in bubble stirred ladles: Part I. Experiments. *Metallurgical Transactions B* 19, 745-754, DOI: https://doi.org/10.1007/BF02650194.

[5] Nakaoka, T., Taniguchi, S., Matsumoto, K. & Johansen, S. T. (2001). Particle size grouping method of inclusion agglomeration and its application to water model experiments. *ISIJ International.* 41, 1103-1111. DOI: https://doi.org/10.2355/isijinternational.41.1103.

[6] Saffman, P.G. & Turner, J.S. (1956). On the collision of drops in turbulent clouds. *Journal of Fluid Mechanics.* 1, 16-30. DOI: https: //doi.org/10.1017/S0022112056000020.

[7] Wang, L., Lee, H. G. & Hayes, P. (1996). Prediction of the optimum bubble size for inclusion removal from molten steel by flotation. *ISIJ International.* 36, 7-16, DOI: https://doi.org/10.2355/isijinternational.36.7.

[8] Schulze, H. J. (1989). Hydrodynamics of bubble-mineral particle collisions. *Mineral Processing and Extractive Metallurgy Review.* 5, 43-76. https://doi.org/10.1080/08827508908952644.

[9] Bouris, D. & Bergeles, G. (1998). Investigation of inclusion re-entrainment from the steel-slag interface. *Metallurgical and Materials Transactions B.* 29, 641-649. DOI:

https://doi.org/10.1007/s11663-998-0099-6.

[10] Strandh, J., Nakajima, K., Eriksson, R. & Jonsson, P. (2005). Solid inclusion transfer at a steel-slag interface with focus on tundish conditions. *ISIJ International.* 45, 1597-1606, DOI: https://doi.org/10.2355/isijinternational.45.1597

[11] Votava, I. & Matiašovský, K. (1973). Measurement of viscosity of fused salts. II. viscosity of molten binary mixtures on the cryolite basis. *Chemical Papers.* 27(5), 582-587.

[12] Suchora-Kozakiewicz, M. & Jackowski, J. (2017). Evaluation of interfacial tension in the liquid aluminum alloy – liquid slag system. *Journal of Casting & Materials Engineering.* 1(1), 11-14. DOI: https://doi.org/10.7494/jcme.2017.1.1.11.

[13] Zhang, L. & Taniguchi, S. (2000). Fundamentals of inclusion removal from liquid steel by bubble flotation. *International Materials Reviews.* 45(2), 59-82.
DOI: https://doi.org/10.1179/095066000101528313.

[14] Żak, P. L., Kalisz, D., Lelito, J., Szucki, M., Gracz, B., & Suchy, J. S. (2015). Modelling of non-metallic particles motion process in foundry alloys. *Metalurgija.* 54(2), 357-360.

[15] Dewing, E.W. (1972). Thermodynamics of the system NaF-AlF3. part III: Activities in liquid mixtures. *Metallurgical Transactions B.* 3, 499-505, DOI:

[16] Dewing, E. (1970). Thermodynamics of the system NaF-AlF3 part I: The equilibrium 6NaF(s) + Al = Na3AlF6(s) + 3Na. *Metall. Transactions.* 1, 1691-1694, DOI: https://doi.org/10.1007/BF02642018.

[17] Ransley, C.E. & Neufeld, H. (1950). The solubility relationships in the Al-Na and Al-Si systems. *Journal of Institute of Metals.* 78, 25-46.

[18] Kvande, H. (1980) Solubility of aluminium in NaF-AlF3-Al2O3 melts. *Light Metals.* 171-182.

[19] Dewing, E.W. (1980). Thermodynamic functions for LiF-AlF3 mixtures at 1293 k. *Metallurgical Transactions B.* 11, 245–249, DOI: https://doi.org/10.1007/BF02668408.

[20] Wang, L.T., Zhang, Q.Y., Deng, C.H. & Li, Z.B. (2005). Mathematical model for removal of inclusion in molten steel by injecting gas at ladle shroud. *ISIJ International.* 45, 1138-1144, DOI: https://doi.org/10.2355/isijinternational.45.1138.

[21] Suchora-Kozakiewicz, M. & Jackowski, J. (2017). The way of estimating interphase tension in the liquid aluminum alloy – liquid slag. *Composites Theory Practice.* 17(2), 73-78.